Method for Precise Analysis of the Metal Package Photomultiplier Single Photoelectron Spectra

January 25, 2000

I.Chirikov-Zorin[1], I Fedorko[2], A. Menzione[3], M. Pikna[2], I. Sýkora[2], and S. Tokár[2]

Abstract

A sophisticated photomultiplier response function was suggested for single photoelectron analysis of the compact metal package photomultiplier spectra. The spectra taken by Hamamatsu R5600 photomultipliers have been analysed by the presented method. The detailed analysis shows that the method appropriately describes the process of charge multiplication in these photomultipliers and can be used to find their basic internal parameters.

[1]Joint Institute for Nuclear Research, 141980 Dubna, Moscow Region, Russia.

[2]Dept. of Nuclear Physics, Comenius University, Mlynska Dolina F1, 84215 Bratislava,Slovakia.

[3]Istituto Nazionale di Fisika Nucleare (INFN),Via Livornese, 582A San Piero a Grado, 56010 Pisa, Italy.

1 Introduction

Photomultipliers (PMTs) are widely used as light detection components of different types of scintillation and Cherenkov detectors (counters, calorimeters, etc.). Some intrinsic spread in characteristic parameters of PMTs, stemming from their multiplicative nature, and their time dependence are among the most serious drawbacks of this type of light detection. Therefore calibration and monitoring of PMT-based spectrometric channels are an inevitable and important part of the experimental setups. Especially important is the absolute calibration, i.e. the measurement of the energy deposited in scintillators in terms of photoelectrons created from the PMT photo-cathode and captured by the PMT first dynode. The reason is that the basic properties of the scintillating detectors (efficiency, energy resolution, etc.) depend on the number of photoelectrons registered by a detector per unit of deposited energy. In addition the study of the PMT intrinsic parameters is inevitable for a correct estimate of the basic characteristics of such PMT based detectors like calorimeters are (the energy to signal conversion factor, etc). An effective mean of these studies is method of the single photoelectron analysis ([1],[2], [3]) In our previous work [1] we presented a method of PMT calibration and monitoring based on deconvolution of pulse height spectra from a low amplitude pulsed light source which lead to the spectra with a few photoelectrons created on PMT photo-cathode. A key point of such a method is the choice of the PMT response function. In the work mentioned above we had employed a response function suggested for high resolution PMTs with traditional structure [4] (phototubes with the linear focusing dynodes, box dynodes, venetian-blind dynodes) and satisfactory results had been achieved.

In this work we present the deconvolution method based on the same principles as before [1] for the new types of ultra compact PMTs with the metal channel dynode system [5]. The compactness of these phototubes makes them attractive for applications in high energy physics experiments where experimental setup compactness is of prime importance. The metal channel PMTs are being extensively investigated in high energy physics experiments as the CDF collaboration for the muon detector R&D [6], where the effect of the photoelectron production on PMT first dynode was reported, and ATLAS collaboration for needs of the hadron calorimeter R&D program [7, 8].

2 Photomultiplier Response

The basic idea of the calibration and monitoring method consists of a deconvolution of the PMT pulse height spectrum and subsequent use of some of the extracted parameters for calibration purposes. The response function must take care of all important PMT processes. In our approach the PMT is treated as consisting of three independent functional parts:

- The photo-detector represented by the photo-cathode, where the input photon flux is converted into electrons,
- The photoelectron optical input system which accelerates and focuses the photoelectron flux onto the first dynode,
- The electron multiplier consisting of a series of secondary emission electrodes (dynodes), which amplifies the initial charge emitted by the photo-cathode.

The PMT response function must take into account peculiarities of the PMT structure, and in our case, we will concentrate on the class of metal package PMTs [5]. The global view of such a PMT is shown in Fig.1, where the structure of a Hamamatsu R5600 PMT is depicted.

The PMT structure can be simplified to two independent stages. The first stage includes the photo-conversion and electron collection and the second one includes the charge amplification through the dynode system.

2.1 Photo-conversion and Electron Collection

A pulsed flux of photons incident on PMT photo-cathode produces photoelectrons via the photo-electric effect. In many cases the number of photons on the photo-cathode is a Poisson distributed variable. In addition to this, the conversion of photons into electrons and their subsequent collection by the dynode system is a random binary process. As a result the distribution of the photoelectrons can be expressed as a convolution of Poisson and binary processes. This gives again a Poisson distribution:

$$P(n, \mu_{pc}) = \frac{\mu_{pc}^n \cdot e^{-\mu_{pc}}}{n!} \tag{1}$$

with μ_{pc} defined as

$$\mu_{pc} = n_{ph} \cdot q \tag{2}$$

where μ_{pc} is the mean number of photoelectrons collected by the dynode system, and q is the quantum efficiency folded with the collection efficiency.

P(n, μ_{pc}) is the probability that n photoelectrons will be collected provided that their mean is μ_{pc}, n_{ph} is the mean number of photons hitting photo-cathode,.

Note that μ_{pc} is a parameter characterising not only the light source intensity but also the photo-cathode quantum efficiency and the PMT dynode collection efficiency, which depends on the voltage applied between the photo-cathode and the first dynode.

2.2 Electron Multiplication

A single photoelectron from the PMT photo-cathode having been focused and accelerated by the electric field, strikes the first dynode and causes a production of the secondary emission electrons. Subsequently, each of them accelerated by inter-dynode potential creates the secondary emission electrons on the second dynode, etc. The charge multiplication process in the dynode system for the R5600 PMT is shown in Fig.2.

An electron avalanche is finally created at the anode resulting in the PMT output charge. The electron avalanche might be described under the following assumptions:

- The emission of secondary electrons is governed by a Poisson law;
- The number of secondaries (n_S) depends on the energy (E) of the incident electron as $n_s = const \cdot E^{\alpha}$, where α is less than 1 (usually $\alpha \approx 0.4 - 0.8$) [4]);
- The energy of secondary electrons is low compared to the energy acquired by the primary from the electric field

All these peculiarities must be considered for the construction of the response function. The PMT response can be easily found in the case that the number of secondary electrons on the first dynode is high ($\geq$ 7). In this case, and in the absence of background processes, the charge distribution for the amplification process initiated by one photoelectron can be approximated by a Gaussian distribution. The distribution for the n photoelectron case is a convolution of n one-photoelectron distributions. This idealised case is obtained by summing those distributions with different starting numbers of photoelectrons, weighted by their occurrence probability [1]:

$$S_{ideal}(x) = \sum_{n=0}^{\infty} \frac{\mu_{pc}^{n} e^{-\mu_{pc}}}{n!} \frac{1}{\sigma_1 \sqrt{2\pi n}} \exp\left(-\frac{(x - nQ_1)^2}{2n\sigma_1^2}\right) \tag{3}$$

where Q_1 is the average charge in the one-photoelectron case and σ_1 is the standard deviation of the one-photoelectron distribution (in $n = 0$ case the limit ($n \rightarrow 0$) delta function $\delta(x)$ should be taken instead of Gaussian).

2.3 Realistic PMT Response Function

The basic drawbacks of the function (3) are the following:

- Background processes are taken into account;
- The one-photoelectron function is assumed to be Gaussian (not true for low values of the secondary emission coefficient on the first dynode);
- No additional processes connected with semi-transparency of the photo-cathode (like photo-electric effect on the first dynode, focusing and acceleration electrodes) are assumed.

All these issues must be addressed to obtain a realistic response function.

2.3.1 Background Processes

In a real PMT various background processes will always occur which will ultimately generate some additional charge (noise). Such noise signal in the anode is generated even in absence of the light signal.

The possible sources of noise are: leakage current, thermo-emission from the photo-cathode and dynodes, optical and ion feedback, external and internal radioactivity, etc. Undesired signals of low amplitude at the PMT output can also arise from the incident light flux. The possible sources of these signals are: the photo-emission from the focusing and accelerating electrodes and from the dynodes, photoelectrons missing the first dynode and its subsequent absorption by the second dynode, etc.

The background processes generate some additional charge and modify the ideal output charge spectrum (3). We split the background processes into two groups:

1. The low charge processes present in each event (e.g. leakage current in the PMT anode circuit, etc.) which are responsible for a non-zero width of the pedestal (the output charge distribution in the case when no photoelectrons were created);

2. The discrete processes, which can, with non-zero probability, accompany the real signal.

Note that with "the real signal" we mean the one corresponding to non-zero number of photoelectrons created from the photo-cathode and collected by the first dynode.

2.3.2 Response Function for the Metal Package PMT

To create a realistic PMT response function we have made a few natural assumptions.

1. The low charge background processes, which will lead to the finite width of pedestal, may be represented by the formula:

$$S_{ped}(x) = \frac{1}{\sqrt{2\pi}\sigma_0} \exp\left(-\frac{(x-Q_0)^2}{2\sigma_0^2}\right) \tag{4}$$

with Q_0 - the pedestal position and σ_0- it's standard deviation.

2. The incident light can create photoelectrons from the PMT photo-cathode, as well as from the first dynode with the occurrence probability for n photoelectrons created from the photo-cathode and k photoelectrons created from the first dynode given by (1) and the mean number of photoelectrons: μ_{pc}- from the photo-cathode and μ_1- from the first dynode.

3. If one or two photoelectrons are collected by the first dynode, then the PMT response is expressed as a sum of responses of secondary electrons created on the first dynode, and for zero and greater than two photoelectrons collected, it is a Gaussian:

$$S_n^{(1)}(x) = \begin{cases} \sum_{m=0}^{\infty} \frac{K_1^m \cdot e^{-K_1}}{m!} \cdot S_m^{(2)}(x) & n = 1 \\ \sum_{m=0}^{\infty} K_1^m e^{-2K_1} \cdot \sum_{l=0}^{m} \frac{1}{(m-l)!l!} \cdot S_m^{(2)}(x) & n = 2 \\ G\left(x,\, Q_0 + nQ_1,\, \sigma_0^2 + n\sigma_1^2\right) & n = 0,\, n \geq 3 \end{cases} \tag{5}$$

Where,

- Q_0, σ_0 are the pedestal and its width;
- Q_1, σ_1 - the multiplication process parameters gain, one photoelectron response standard deviation;
- K_1 - the secondary emission coefficient of the first dynode;
- $S_m^{(2)}(x)$ is the PMT response for the multiplication process started by an electron from the first dynode;
- $G\left(x, Q, \sigma^2\right)$ is a Gaussian distribution with the mean value of Q and dispersion σ^2:

Remark. One photoelectron response is not symmetric and σ_1 can be different from the standard deviation of the real one photoelectron response. By σ_1 we mean the quantity:

$$\sigma_1 = \frac{\sigma_n^{real}}{\sqrt{n}} \tag{6}$$

Where σ_n^{real} is the standard deviation in the case that the number of captured photoelectrons is high enough to give symmetric Gaussian response, practically n (≥ 3) is sufficient.

For the response of the photoelectrons created on the first dynode the expression analogous to (5) can be written:

$$S_k^{(2)}(x) = \begin{cases} \delta(x) & k = 0 \\ \sum_{m=0}^{\infty} \frac{K_2^m \, e^{-K_2}}{m!} G\left(x,\, Q_0 + mQ_3,\, \sigma_0^2 + \sigma_3^2\right) & k = 1 \\ G\left(x,\, Q_0 + kQ_2,\, \sigma_0^2 + \sigma_2^2\right) & k \geq 2 \end{cases} \tag{7}$$

where k is the number of the photoelectrons created on the first dynode, K_2 is the secondary emission coefficient of the second dynode, $Q_2 = Q_1/K_1$ is the mean charge at the anode initiated by one electron from the first dynode and σ_2 is corresponding standard deviation, $Q_3 = Q_2/K_2$ is the mean charge at the anode initiated by one electron from the second dynode and σ_3 is its standard deviation.

All other processes can be neglected for the moment. The output charge spectrum for the case in which n photoelectrons have been created on the photo-cathode and k on the first dynode, can be expressed as the following convolution:

$$S_{real}(x) = \sum_{n,k=0}^{\infty} \frac{\mu_{pc}^n \, e^{-\mu_{pc}}}{n!} \cdot \frac{\mu_1^k \, e^{-\mu_1}}{k!} \cdot \int dx' \, S_n^{(1)}(x') \cdot S_k^{(2)}(x - x') \tag{8}$$

where

- μ_{pc} - the light source intensity expressed in number of photoelectrons captured by the PMT dynode system;
- μ_1 - the number of photoelectrons created on the first dynode and captured by the following dynode system.

The formula shown above presumes that in the case of two or less photoelectrons collected by the first dynode the PMT response is not a Gaussian. In this case the response is expressed as a sum

of the responses corresponding to different numbers of electrons collected by the second dynode and weighted by the corresponding Poisson factors - the number of secondaries created on the dynode by one electron is governed by Poisson statistics. From the simulation of the R5600 response (see bellow) we can conclude, that at least at high gain (in our case at the PMT voltage $\geq$ 800 V), it is sufficient to expand the PMT response in case when 1 or 2 photoelectrons are captured. The convolution

$$\widetilde{S}_{nk}(x) = \int dx'\, S_n^{(1)}(x') \cdot S_k^{(2)}(x - x') \tag{9}$$

can be expressed as follows:

$$\widetilde{S}_{nk}(x) = \begin{cases} \sum_{m=0}^{\infty} \frac{K_1^m\, e^{-K_1}}{m!} G\left(x,\, Q_0 + (m+k)\cdot Q_2,\, \sigma_0^2 + (m+k)\cdot \sigma_2^2\right) & n = 1 \\ \sum_{m=0}^{\infty} K_1^m\, e^{-2K_1} \sum_{l=0}^{m} \frac{1}{(m-l)!\, l!} G\left(x,\, Q_0 + (m+k)\cdot Q_2,\, \sigma_0^2 + (m+k)\cdot \sigma_2^2\right) & n = 2 \\ G\left(x,\, Q_0 + nQ_1 + kQ_2,\, \sigma_0^2 + n\sigma_1^2 + k\sigma_2^2\right) & n = 0,\, n \geq 3 \end{cases} \tag{10}$$

The response function $S_{real}(x)$ can be further generalised if the effect of "fly through" photoelectrons are taken into account. These are photoelectrons from the photo-cathode collected on the second dynode instead in the first one. In this case the PMT response function reads:

$$S_{real}(x) = \sum_{n,k=0}^{\infty} \frac{\mu_{pc}^n\, e^{-\mu_{pc}}}{n!} \cdot \frac{\mu_1^k\, e^{-\mu_1}}{k!} \cdot \sum_{i=0}^{n} \begin{pmatrix} n \\ i \end{pmatrix} w_2^i (1 - w_2)^{n-i} \int dx'\, \widetilde{S}_{n-i,k}(x') \cdot \widetilde{S}_i^{\,(2)}(x - x') \tag{11}$$

where

- w_2 is the probability that a photoelectron created on the photo-cathode will be captured by the second dynode (and not by the first one);
- $\widetilde{S}_i^{(2)}$is a response corresponding to i photoelectrons originating from the photo-cathode and collected on the second dynode.

2.3.3 The Limit Spectrum

For many applications it is important to consider the limit of the real spectrum (8) for high intensity light sources ($\mu_{pc} \rightarrow \infty$). At large values of μ_{pc} and μ_1 the Poisson distributions present in (8)

become Gaussian:

$$\frac{\mu_{pc}^{n}\ \exp(-\mu_{pc})}{n!}\ \overrightarrow{\mu_{pc}\ \to\ \infty}\ \frac{\exp\left(-\frac{(n-\mu_{pc})^2}{2\mu_{pc}}\right)}{\sqrt{2\pi\mu_{pc}}} \tag{12}$$

$$\frac{\mu_{1}^{k}\ \exp(-\mu_{1})}{k!}\ \overrightarrow{\mu_{1}\ \to\ \infty}\ \frac{\exp\left(-\frac{(k-\mu_{1})^2}{2\mu_{1}}\right)}{\sqrt{2\pi\mu_{1}}} \tag{13}$$

and the PMT response from n photoelectrons from the photo-cathode and k photoelectrons from the first dynode can be represented by a Gaussian:

$$\widetilde{S}_{nk}(x)\ \overrightarrow{\mu_{pc}\ \to\ \infty}\ G\left(x,\ Q_0 + nQ_1 + kQ_2,\ \mu_{pc}\sigma_1^2 + \mu_1\sigma_2^2\right) \tag{14}$$

As in the summation present in (8) only n from $\left(\mu_{pc} - \sqrt{\mu_{pc}},\ \mu_{pc} + \sqrt{\mu_{pc}}\right)$ and k from $\left(\mu_1 - \sqrt{\mu_1},\ \mu_1 + \sqrt{\mu_1}\right)$ will effectively contribute. Replacing in (8) the summation over n and k by integration, the PMT response function goes to the limit spectrum:

$$S_{real}(x)\ \ \overrightarrow{\mu_{pc}\ \to\ \infty}\ \ S_{\infty}(x) = \frac{1}{\sqrt{2\pi}\sigma_{\infty}}\exp\left(\frac{(x - Q_0 - Q_{\infty})^2}{2\sigma_{\infty}^2}\right) \tag{15}$$

where

$$Q_{\infty} \quad = \quad \mu_{pc}Q_1 + \mu_1 Q_2 = \mu_{pc}Q_1\left(1 + \frac{\varepsilon}{K_1}\right) \tag{16}$$

$$\sigma_{\infty} \quad = \quad \sqrt{\sigma_0^2 + \mu_{pc}\left(\sigma_1^2 + Q_1^2\right) + \mu_1\left(\sigma_2^2 + Q_2^2\right)}\ \ \overrightarrow{\epsilon < 0.1}\ \ \sqrt{\mu_{pc}\left(\sigma_1^2 + Q_1^2\right)} \tag{17}$$

$$\tag{18}$$

where $\epsilon = \frac{\mu_1}{\mu_{pc}}$ and $K_1 \equiv$ secondary emission coefficient on the first dynode.

It is useful to find a relation between the limit spectrum parameters (Q_{∞}, σ_{∞}) and the mean number of photoelectrons (μ_{pc}, μ_1). From (16) and (18) it follows:

$$\mu_{pc} \quad = \quad f_{pmt}\cdot\frac{Q_{\infty}^2}{\sigma_{\infty}^2} \tag{19}$$

$$f_{pmt} = \frac{\sigma_1^2 + \epsilon\sigma_2^2 + Q_1^2\left(1+\frac{\epsilon}{K_1^2}\right)}{Q_1^2\left(1+\frac{\epsilon}{K_1}\right)^2} \longrightarrow 1 + \frac{\sigma_1^2}{Q_1^2} \quad (20)$$

The last relation is justified if the effect on the first dynode is small ($\epsilon < 0.1$). The factor f_{pmt} depends on the single photoelectron parameters (one photoelectron resolution) of the PMT in question, and its value is different from one. Typical values of f_{pmt} are expected to vary between 1.15 to 1.50 .

2.3.4 Relation Between Amplification Process Parameters

A realistic PMT response function like the one given by (8) or (11) is always expressed through several parameters: Q_0, σ_0, Q_1, σ_1, Q_2, σ_2, μ_{pc} and μ_1 (in case of the relation (11) the additional parameter w_2 is present). Some of the parameters are clearly independent, as Q_0 and σ_0 (defining pedestal position and width, μ_{pc} and μ_1 - characterising the light source intensity in combination with photon to electron conversion at the photo-cathode and first dynode. The other parameters Q_1, σ_1, Q_2, σ_2 , characterising the charge multiplication process in the dynode system, are not fully independent. It is important to know what the relationships between them are.

Starting with the assumption that the PMT has an N stage dynode system and that one electron hitting the i^{th} dynode will create an average k_i of secondary electrons. If we denote as Q_1 the mean anode charge initiated by one electron captured by the first dynode, then it is easy to express Q_1 via dynode coefficients k_i and elementary charge e :

$$Q_1 = e \cdot k_1 \cdot k_2 \cdots k_N = e \cdot \prod_{i=1}^{N} k_i \quad (21)$$

The variance σ_1^2 of the anode charge initiated by one electron can be expressed as [9]:

$$\sigma_1^2 = Q_1^2\left(\left(\frac{\delta_1}{k_1}\right)^2 + \frac{1}{k_1}\left(\frac{\delta_2}{k_2}\right)^2 + \ldots + \frac{1}{k_1 k_2 \cdots k_N}\left(\frac{\delta_N}{k_N}\right)^2\right) \quad (22)$$

Where δ_i $(i = 1, \ldots, N)$ is the standard deviation of the number of secondary electrons created from the i^{th} dynode by one electron.

The formulae (21) and (22) can be straightforwardly generalised for the case when the charge multiplication starts from the j^{th}dynode:

$$Q_j = e \cdot k_j \cdot k_{j+1} \cdots k_N = e \cdot \prod_{i=j}^{N} k_i \quad (23)$$

and

$$\sigma_j^2 = Q_j^2 \left(\left(\frac{\delta_j}{k_j} \right)^2 + \frac{1}{k_j} \left(\frac{\delta_{j+1}}{k_{j+1}} \right)^2 + \ldots + \frac{1}{k_j k_{j+1} \cdots k_N} \left(\frac{\delta_N}{k_N} \right)^2 \right) \tag{24}$$

where Q_j and σ_j are mean charge and corresponding standard deviation for the case when the charge multiplication starts from j^{th} dynode.

The validity of the relation (22) is shown for the case $N = 2$ in Appendix 1 and can be easily generalised for the general case of N dynodes.

Simplification of the formulae (22) and (24) can be achieved if we assume that the standard deviations δ_i are governed by a Poisson law:

$$\delta_i = \sqrt{k_i} \tag{25}$$

Assuming (25) the relation between σ_j and Q_j reads

$$\sigma_j^2 = Q_j^2 \left(\frac{1}{k_j} + \frac{1}{k_j k_{j+1}} \ldots + \frac{1}{k_j \cdots k_N} \right) \tag{26}$$

At a fixed voltage the factor in brackets is a PMT constant which can be determined as the PMT base repartition. If the repartition is $1 : 1 : \ldots : 1$, then for all dynodes $k_i = k$ and the formula (26) becomes

$$\sigma_j^2 = Q_j^2 \left(\frac{1}{k} + \frac{1}{k^2} \ldots + \frac{1}{k^{N-j+1}} \right) \tag{27}$$

where $j = 1, 2, ..., N-1$.

Now instead of 4 parameters $Q_1, \sigma_1, Q_2, \sigma_2$ we have only two independent parameters (Q_1, k). Moreover, the dynode multiplication coefficient can be found independently from the average gain G using relation:

$$G = k^N = Q_1/e \tag{28}$$

It should be stressed that the relations like (26) and (27) are valid only for an ideal case. In a real case inhomogeneities of various kinds (like the dynode surface inhomogeneity, collection inefficiency, etc.) will make the value of standard deviation broader than in the ideal case. In our analysis we usually use three of the parameters: Q_1, σ_1, $k_1 = Q_1/Q_2$ finding the fourth of them on the basis of (26). On the other hand a possibility to free all four parameters has been conserved as well as a possibility to fix all possible parameters.

2.3.5 Secondary Emission Coefficients

The secondary emission coefficient of a dynode can be expressed [10] as

$$n = a \cdot E^{\alpha}$$

Where E is the incident electron energy, α is a material dependent coefficient and a is a coefficient determining the absolute gain of the PMT. The energy of the electron is essentially determined by inter-dynode voltage as the secondary electron is created with low energy (as compared to the energy acquired in the inter-dynode electric field). Therefore the secondary emission coefficient of the i^{th} dynode is

$$n_i = \gamma U_i^{\alpha} = \gamma \left(\frac{U}{\sum_{j=1}^{N+1} r_j} \right)^{\alpha} r_i^{\alpha} \tag{29}$$

Where U_i is the inter-dynode voltage (between dynode $i-1$ and i, U is the overall voltage between photo-cathode and anode, α is as before and γ is a coefficient analogous to a, r_i $(i = 1, \ldots N+1)$ is the voltage repartition and N is the number of dynodes. Using (29) the PMT gain reads

$$G = \prod_{i=1}^{N} n_i = \frac{\gamma^N \cdot \prod_{i=1}^{N} r_i^{\alpha}}{\left(\sum_{i=1}^{N+1} r_i \right)^{\alpha N}} \cdot U^{\alpha N} \tag{30}$$

If the repartition is fixed, then the gain G is an exponent function of the voltage U and the formula (30) can be used to find the exponent α.

3 Results of Analysis

To verify the response function we took and analysed a series of faint light (a few photoelectrons) spectra under different conditions. These spectra were analysed by means of the response function (8), for the eight dynode R5600 Hamamatsu photomultipliers. The results of the analysis are summarised below.

4 Experimental Setup

Our analytical method based on the deconvolution of the LED spectra using the response function (8) was tested on the experimental data. The block diagram of the experimental setup is shown in Fig. 3. The fast AlGaAs LED HLMP8100 ("Hewlet Packard") was used as a pulsed light source. The LED was driven by a pulse generator (GEN) with a short pulse width($\approx 10\ n\ sec$). An optical fiber was used to transmit light from the LED to the PMT. The photon flux incident on the photo-cathode was tuned by changing the supply voltage to the LED. The analog signal from the PMT was amplified by a preamplifier Model 777 "Philips Scientific" and measured by an ADC (LeCroy 2249A). The width of the gate signal was 80 ns. The output information from the ADC was read by means of PC computer.

4.1 Dependence of the Output Spectrum Parameters on the PMT Voltage.

To find the dependence of the basic parameters on the voltage applied to the PMT, we took the spectra with the same pulsed light source intensity but at different high voltages. The results for the R5600 are shown in Tables 1 and 2 and in Figs. 4 and 5. In Table 1 the deconvoluted parameters of the spectra taken at different PMT voltages are shown for the case when the first dynode secondary emission coefficient K_1 is calculated from Q_1 using the relation (23). Table 2 presents the results of analysis of the same spectra but for the case when K_1 is independent of Q_1 . In Fig. 4 the deconvoluted spectrum taken at $1000\,V$ is shown . In Fig. 5a-d the essential part of the deconvoluted spectra taken at 800 V, 850 V, 900 V and 950 V are shown in linear scale. We can clearly see from these figures the presence of the first dynode effect (the first peak after pedestal). As will be shown below, this effect can be interpreted as caused by the photo-electric effect on the first dynode. It can be seen from Table 1,2 and Fig. 4, 5, the parameter Q_1 (essentially gain expressed in the ADC channels) increases with the voltage as expected. The first dynode secondary emission coefficient K_1 also shows the same behaviour. A small increase in the mean number of photoelectrons (μ_{pc}) with voltage is seen. This effect can be explained by the fact that even at voltages higher than the plateau threshold, the voltage at which collection efficiency reaches

its plateau, there is an increase of the photoelectron collection efficiency. This effect is also observed at photo-cathode current measurement in the mode with the continuous light source [8] as a slight increase of photo-cathode sensitivity with voltage between photo-cathode and first dynode. This is an edge effect which can be especially visible for the PMTs with a small effective photo-cathode, as the effect should be proportional to the ratio of the photo-cathode circumference and surface, i.e. it should be proportional to 1/R, where R is the photo-cathode radius. From Tables 1,2 we also see that the ratio μ_1/μ_{pc} is essentially stable. The fluctuations of this ratio could arise from the definition of the first dynode peak area. This systematic error found from the μ_1/μ_{pc} fluctuation is about 5-7%. From the dependence of parameter Q_1 on high voltage, the secondary emission exponent α can be found. We fit Q_1 data from Table 2 with formula (30) and obtained $\alpha = 0.874 \pm 0.007$. The result of this fit is shown in Fig. 6. The coefficient is important in the case when a non-uniform voltage divider is used.

4.2 Output Spectrum Parameters vs. First Dynode Voltage.

To understand the nature of the first dynode effect we have taken a series of spectra with different voltages between first dynode and photo-cathode (U_1). The voltage U_1 is a sensitive parameter that enables us to distinguish between the photo-electric effect on the first dynode and direct capture of photoelectrons by the second dynode. In case of the latter effect a photoelectron created from the photo-cathode is missing the first dynode and is captured directly by the second dynode. If the first dynode effect is caused by the photoelectrons directly captured by second dynode, then the position of the first dynode peak (Q_2) will move with the voltage U_1 as $Q_2 \sim (U_1 + U_2)^\alpha$, while if it is caused by the photo-electric effect on first dynode, then this peak will not move, as in this case $Q_2 =\sim U_2^\alpha$ and U_2 does not change. To exclude possible systematic uncertainties (determining the first dynode peak area, etc.) we fixed the secondary emission coefficient on the first dynode K_1 via formula (29). The results of analysis are presented in Fig. 7 and Table 3 from where it can be seen that the position of the first dynode peak (Q_2) does not move with the voltage U_1. In case of the second dynode direct capture effect, more than 50 % increase of Q_2 is expected when U_1 is increased form *139 V* to *228 V*. Therefore we conclude that the first dynode peak is caused

mainly by the photo-electric effect on first dynode. From the results we also see that χ^2 of the fit increases with increasing voltage U_1(increasing divider non-uniformity). Fig.7 neatly shows that the discrepancy is in the region of small amplitudes (left side of the one photoelectron distribution), where an excess is of real events over the expected ones is observed. The discrepancy at high values of voltage between the photo-cathode and first dynode can be caused by some presence of direct capture of photoelectrons by second dynode and the above mentioned edge effect. In the former case, the photoelectrons from photo-cathode are captured by second dynode and are accelerated by bigger voltage than the photoelectrons from first dynode. It will lead to an enhanced signal if compared with that initiated by the photoelectrons from the first dynode. In the latter case, the photoelectrons from photo-cathode may produce less secondary electrons on first dynode and that would lead to an enhanced left tail of the one-photoelectron distribution.

4.3 Comparison of the experimental spectra with the simulation.

For better understanding of the observed spectra and results of their analysis we compared them with the spectra obtain with the simulation. Details of the code were published elsewhere [13]. Here we only give the main features of the code:

- Photo-conversion is governed by Poisson law and can occur on photo-cathode and on first dynode.
- Charge multiplication in PMT dynode system is also governed by Poisson law.
- Possible inhomogeneity of dynode system, i.e dependence of dynode secondary emission coefficient on place of incidence, has been introduced into the code.
- Direct capture of photo-cathode electrons by second dynode has been included.

First of all we simulated an 8-staged PMT assuming that the charge multiplication process is an ideal one, i.e. production of secondaries obeys Poisson law, no inhomogeneities are present, photoelectrons are created only on photo-cathode and collection efficiency of dynode system is 100%. We carried out the simulation for two PMT gains corresponding to two voltages of the tested R5600

PMT - 850 V and 1000 V. The main purpose of these simulation was to investigate how the form of PMT response depends on number of photoelectrons initiating it. The results are presented in Fig. 8 - 9, where the charge distributions initiated by $n = 0, 1, 2, 3, 4$ and 6 photoelectrons are shown for the two different gains. We can conclude that for gains greater than 10^6 the "idealised" PMT response is symmetric(Gaussian) if charge distribution is initiated by 3 or more photoelectrons. One can expect that inhomogeneities (in a real case) will not change this fact dramatically, i.e. our choice to expand the PMT response, in cases when it is initiated by 1 or 2 photoelectrons, is justified.

In a second phase we have tried to reproduce a real response of the tested PMT. In Fig.10 the experimental spectra taken by the R5600 PMT taken at 850 V and 1000 V have been compared with those obtained in the simulation . The spectra were simulated under two different sets of conditions. In the first case an idealised response of PMT was assumed - neither direct capture of photoelectrons by second dynode nor dynode inhomogeneity has been included. In the second case more realistic conditions were treated - both above mentioned effects have been included. The spectra obtained for an "idealised" (dotted line) conditions do not reproduce the experimental data properly. On the other hand the spectra obtained under a more realistic conditions (dashed line) are in an excellent agreement with the observed ones (thick line). This good agreement was achieved for 17% dynode inhomogeneity and approximately 30% direct capture effect if compared with the photo-electric effect on first dynode. It should be stressed that the second dynode direct capture effect can "arise" as a result of systematics connected with behaviour of left tail of one photoelectron response or right tail of the first dynode photoelectron response. In any case it appears that the dominant role in the first dynode effect plays the photo-conversion on the first dynode.

It should be noted that at the simulation input we used as input parameters only: the PMT gain, voltage repartition ($1 : 1 : ... : 1$), ADC resolution (10 bits, 0.25 pC/channel) and position of pedestal.

5 Conclusions

We present the results showing that the deconvolution method, for analysis of single photoelectron spectra of metal package photomultipliers, works well, at least for the class of the above mentioned PMTs.

The PMT response function employed in this method describes in an adequate way processes in the metal package photomultiplier and enables to watch also subtle effects as the photo-conversion on first dynode and/or direct capture of photoelectrons by second dynode.

The method uses only the elementary physical principles and therefore can be easily adapted to other types of photomultipliers.

Our method enables to find important PMT parameters like the position of the charge distribution initiated by one photoelectron (PMT gain), its standard deviation, etc.(c.f. part 2.3.4). On the basis of these parameters we can calculate the PMT access factors needed in finding the relation between the mean numbers of photoelectrons and parameters of an experimental spectrum with high input light signal (19,20), and it enables us to calculate the energy-to-signal conversion factor (number of photoelectrons per GeV) for PMT based calorimeters.

The method can be used as a calibration and monitoring tool for studying stability in time of a photomultiplier using the gain (parameter Q_1).

6 Acknowledgements

The authors want to thank S. Leone (INFN Pisa) for an accurate reading of the manuscript and for valuable remarks and P. Strmen (Comenius Univ., Bratislava) for technical help.

Appendix. Fluctuations in a Two Dynode System

In the case of a two-dynode system the anode charge can be expressed as

$$q = \sum_{i=1}^{q_1} q_2^{(i)} \tag{31}$$

Where q_1 is the number of electrons created from the first dynode and q_2^i is the number of electrons created from the second dynode by i^{th} electron from the first dynode. The mean value of charge q is easy to find:

$$\bar{q} = E\left(\sum_{i=1}^{q_1} q_2^{(i)}\right) = \sum_{m=0}^{\infty} P_m^{(1)} \sum_{i=1}^{m} E\left(q_2^{(i)}\right) = \sum_{m=0}^{\infty} P_m^{(1)} m k_2 = k_1 k_2 \tag{32}$$

Where E is the expected value, $P_m^{(1)}$ is the probability to have m electrons created from the 1^{st} dynode. We used the fact that each of the 1^{st} dynode electrons creates from the 2^{nd} dynode the same average number of electrons k^2.

The dispersion σ_q^2 can be expressed as

$$\sigma_q^2 = E\left(q^2\right) - k_1^2 \dot{k}_2^2 \tag{33}$$

Where

$$\begin{aligned} E\left(q^2\right) &= E\left(\sum_{i,j=1}^{q_1} q_2^{(i)} q_2^{(j)}\right) = \sum_{m=0}^{\infty} P_m^{(1)} \sum_{i,j=1}^{m} E\left(q_2^{(i)} q_2^{(j)}\right) \\ &= \sum_{m=0}^{\infty} P_m^{(1)} \left(m\bar{q_2^2} + m(m-1)k_2^2\right) = k_1 \bar{q_2^2} + k_2^2 \bar{q_1^2} - k_1 k_2^2 = k_1 \sigma_2^2 + k_2 \bar{q_1^2} \end{aligned} \tag{34}$$

Combining (33) and (34) we have

$$\sigma_q^2 = (k_1 k_2)^2 \left[\left(\frac{\sigma_1}{k_1}\right)^2 + \frac{1}{k_1}\left(\frac{\sigma_2}{k_2}\right)^2\right] \tag{35}$$

Generalisation of (35) to the general case of N dynodes is straightforward and leads to the relation (22).

7 Tables

Table 1: Dependence of the R5600 PMT output spectrum parameters on the voltage applied to the PMT. The fitting function (8) has been applied with the ratio $\sigma_3/Q_3 = \sigma_2/Q_2$ and K_1 calculated from Q_1.

U	800 V	850 V	900 V	950 V	1 kV
Q_0	13.53± 0.022	13.59 ±0.017	13.59±0.015	13.45±0.018	13.54 ±0.015
σ_0	0.47±0.017	0.47 ±0.015	0.49 ±0.015	0.67 ±0.02	0.53±0.017
Q_1	15.20 ±0.04	23.32 ±0.09	35.24 ±0.26	50.52 ±0.37	72.76 ±0.63
σ_1	7.80 ±0.16	11.32 ±0.23	16.92 ±0.31	24.73 ±0.47	32.04 ±0.60
K_1	5.74	5.97	6.23	6.58	7.06
σ_2	1.60 ±0.06	2.40 ±0.09	3.07 ±0.08	5.55 ±0.26	6.10 ±0.13
μ_{pc}	1.446 ±0.009	1.459 ±0.010	1.466 ±0.015	1.520 ±0.014	1.519 ±0.017
μ_1	0.832 ±0.035	0.867 ±0.03	0.892 ±0.025	0.883 ±0.024	0.949 ±0.023
χ^2	77.9 / 126	134.8 / 181	260.0 / 287	413.7/ 388	533.0 / 493
μ_1/μ_{pc}	57.5 %	59.4 %	60.8 %	58.1 %	62.5 %

Table 2: Dependence of the R5600 PMT output spectrum parameters on the voltage U applied to the PMT. The fitting function (8) has been applied with the ratio $\sigma_3/Q_3 = \sigma_2/Q_2$ and K_1 independent of Q_1.

U	800 V	850 V	900 V	950 V	1 kV
Q_0	13.55± 0.021	13.59 ±0.017	13.59±0.015	13.45±0.018	13.54 ±0.015
σ_0	0.47±0.017	0.47 ±0.014	0.49 ±0.015	0.67 ±0.02	0.53±0.017
Q_1	15.13 ±0.17	23.18 ±0.22	35.17 ±0.26	50.48 ±0.38	72.63 ±0.61
σ_1	7.87 ±0.16	11.46 ±0.24	17.00 ±0.30	24.75 ±0.48	32.19 ±0.61
K_1	5.53 ±0.14	5.80 ±0.11	6.33 ±0.09	6.70 ±0.09	7.06 ±0.08
σ_2	1.62 ±0.07	2.46 ±0.10	3.10 ±0.08	5.92 ±0.25	6.16 ±0.13
μ_{pc}	1.450 ±0.023	1.464 ±0.019	1.468 ±0.015	1.521 ±0.015	1.520 ±0.012
μ_1	0.804 ±0.037	0.841 ±0.03	0.879 ±0.025	0.880 ±0.025	0.936 ±0.023
χ^2	73.9 / 125	125.1 / 180	258.2 / 286	413.3/ 387	530.6 / 492
μ_1/μ_{pc}	55.4 %	57.4 %	59.9 %	57.9 %	61.6 %

Table 3: Dependence of the $R5600$ PMT parameters vs. the voltage between photo-cathode and 1^{st} dynode is U_1 (changed from $139\,V$ to $228\,V$). The voltage between the 1^{st} dynode and anode was fixed at $861\,V$. K_1 is fixed using formula (29) with secondary emission exponent $\alpha = 0.87$ and voltage repartition: $U_1 : \ldots 115 : 115 : 55$; the last voltage in this ratio is th voltage between the last dynode and anode.

U_1	139 V	185 V	205 V	228 V
Q_0	11.57 ± 0.020	11.65 ±0.019	11.66 ±0.018	11.59 ±0.013
σ_0	0.66 ±0.013	0.65 ±0.014	0.66 ±0.013	0.48 ±0.014
Q_1	82.02 ±0.46	102.92 ±0.55	112.15 ±0.61	123.08 ±0.69
σ_1	39.81 ±0.72	47.53 ±0.95	52.98 ±1.05	56.98 ±1.17
K_1	6.49	8.31	9.08	9.97
σ_2	8.25 ±0.16	10.72 ±0.17	12.07 ±0.17	12.08 ±0.14
μ	1.254 ±0.01	1.294 ±0.010	1.276 ±0.010	1.269 ±0.010
μ_1	0.601 ±0.013	0.583 ±0.013	0.555 ±0.013	0.551 ±0.014
χ^2	751.6 / 549	729.7 / 670	907.2 / 681	1464.5 / 732

List of Figures

1 The overall view of a Hamamatsu R5600 photomultilier. 27

2 Charge multiplication process in the metal channel dynode photomultiplier. 27

3 Block scheme of the experimental setup for the measurement of single photoelectron spectra. 28

4 The deconvoluted LED spectrum taken at 1000 V by a Hamamatsu R5600 photomultilier. The first dynode secondary emission coefficient K_1 is treated as an independent parameter. 29

5 The deconvoluted LED spectra taken at 800 V, 850 V,900 V, and 950 V by a Hamamatsu R5600 photomultiplier. The same conditions are valid as in the case of the spectrum in Fig. 4. 30

6 Dependencies of the gain (parameter Q_1) on voltage for the R5600 photomultiplier 31

7 Deconvoluted LED spectra taken at different first dynode voltages (139 V, 185 V, 205 V, and 228V) by a Hamamatsu R5600. The voltage between the first dynode and anode was fixed at 861 V. 32

8 The simulated PMT responses at 850 V initiated by different number of photoelectrons - $n = 0, 1, 2, 3, 4$ and 6. 33

9 The simulated PMT responses at 1000 V initiated by different number of photoelectrons - $n = 0, 1, 2, 3, 4$ and 6. 34

10 The spectra taken at 850 V and 1000 V taken by the R5600 PMT(black line) are compared with the simulated ones 35

References

[1] E. H. Bellamy, I. Chirikov-Zorin, S. Tokar, et al,Absolute Calibration and Monitoring of a Spectrometric Channel Using a Photomultiplier, Nucl Instrum Meth A339,468-476(1994)

[2] Response function for Analysis of the Metal Package Photomultiplier Single Photoelectron Spectra. By: S. Tokar, I. Sykora, M. Pikna, I. Chirikov-Zorin, J.A. Budagov, and A. Menzione, Acta Physica Univ. Comenianae,Vol. XL(1999) 105-122

[3] ATL-TILECAL-99-005 (ATL-COM-TILECAL-99-004), Single Photoelectron Spectra Analysis for the Metal Package Photomultiplier, by: S. Tokar, I. Sykora, M. Pikna, I. Chirikov-Zorin, and A. Menzione, 16 Feb 1999, CERN

[4] Photomultiplier Tubes, principles an applications (Handbook), Phillips Photonics, 1994 France

[5] Y. Yoshizawa, J.Takeuchi, The latest vacuum photo-detector, Nucl Instrum Meth A387 (1997) p. 33

[6] Ju. A. Budagov et al., Long Scintillation Counters with the Shift-Spectrum Fiber Light Guides, JINR, 13-98-304,DUBNA (1998)

[7] ATLAS Collaboration, ATLAS Technical Proposal for a General-Purpose pp experiment at the Large Hadron Collider, CERN/LHCC/ 94-93, CERN, Geneva, Switzerland.

ATLAS Collaboration, ATLAS TILE Calorimeter Technical Design Report, CERN/LHCC/96-42, ATLAS TDR 3, 1996, CERN, Geneva, Switzerland.

[8] a) ATL-TILECAL-98-156 . (ATL-L-PN-156) . Measurement of 20 Hamamatsu R-5900 Photomultiplier Tubes for ATLAS TileCal Module-0 . by: Ames,E ; et al. - 23 Mar 1998

b) ATL-TILECAL-98-152 . (ATL-L-PN-152) . Light yield of the 1997 Extended Barrels Module 0 from Cs data with nominal PMT settings . by: S.Bravo and M.Delfino ; - 23 Mar 1998

c) ATL-TILECAL-98-148 . (ATL-L-PN-148) . Technical characteristics of the prototype of the TILECAL photomultipliers test-bench . by: M.Crouau G.Montarou D.Rey ; - 23 Mar 1998

d) ATL-TILECAL-97-131 . (ATL-L-PN-131) . Study of the light produced in PMT/light guide region of Tile barrel Module 0 . by: Henriques,A ; Nessi,M ; Poulsen,U ; - 28 Nov 1997

e) ATL-TILECAL-97-129 . (ATL-L-PN-129) . Characterisation of 8-stages Hamamatsu R5900 photomultipliers for the TILE calorimeter . by: Crouau,M ; Grenier,P ; Montarou,G ; Poirot,S ; Vazeille,F ; - 20 Oct 1997

f) ATL-TILECAL-97-128 . (ATL-L-PN-128) . Addendum on the estimation of Module 0 PMT 480 nm quantum efficiency . by: G.Montarou ; - 20 Oct 1997

g) ATL-TILECAL-97-125 . (ATL-L-PN-125) . Characterisation of EMI 9112A photomultipliers at Valencia for the ATLAS Tile Calorimeter by: Castillo,V ; Chiron,L ; Fassi,F ; Ferrer,A ; Gil,I ; Gonzalez,S ; Higon,E ; Romance,J.B ; - 20 Oct 1997

h) ATL-TILECAL-97-120 . (ATL-L-PN-120) . Light produced in the Fibre bundle/Light guide/PMT region of the Tile Calorimeter prototype . by: Di Girolamo,B ; Henriques,A ; Maio,A ; Santos,J ; Varanda,M ; - 25 Jun 1997

i) ATL-TILECAL-97-117 . (ATL-L-PN-117) . Study of the charge spectra generated by photomultipliers . by: Cavasinni,V ; et al. - 06 Jun 1997

j) ATL-TILECAL-97-115 . (ATL-L-PN-115) . An estimation of Module 0 R5900 PMT quantum efficiency . by: Montarou,G ; - 10 Apr 1997

k) ATL-TILECAL-97-108 . (ATL-L-PN-108) . Characterisation of the Hamamatsu 10-stages R5900 photomultipliers at Clermont for the TILE calorimeter . by: Bouhemaid,N ; Crouau,M ; Gil Botella,A ; Gonzalez de la Hoz ; Grenier,P ; Montarou,G ; Muanza,G.S ; Poirot,S ; Vazeille,F ; - 28 Apr 1997

l) ATL-TILECAL-96-097 . (ATL-L-PN-97) . Characterization of the new R5900 Hamamatsu photomultiplier in Pisa . by: Beschastnov, P ; Cavasinni, V ; Cologna, S ; Del Prete, T ; Di Girolamo, B ; Mazzoni, E ; - 09 Dec 1996

m) ATL-TILECAL-96-083 . (ATL-L-PN-83) . Results of test linearity of 10-stages and 8-stages R5900 PMTS . by: Crouau, M ; Garnier, E ; Montarou, G ; - 13 Sep 1996

n) ATL-TILECAL-94-041 . (ATL-L-PN-41) . The Tilecal 3-in-1 PMT Base concept and the PMT block assembly . by: Ajaltouni, Z ; et al. - 06 Dec 1994

[9] ATL-TILECAL-97-108 . (ATL-L-PN-108) . Characterization of the Hamamatsu 10-stages R5900 photomultipliers at Clermont for the TILE calorimeter . by: Bouhemaid,N ; Crouau,M ; Gil Botella,A ; Gonzalez de la Hoz ; Grenier,P ; Montarou,G ; Muanza,G.S ; Poirot,S ; Vazeille,F ; - 28 Apr 1997

[10] G. Barbiellini, A.Martins, F.Scuri, A simulation study of the behavior of fine photomultipliers in magnetic field, Nucl Instrum Meth., A362(1996) p. 245

[11] Application Software Group, CERN Program Library, 1995, CERN, Geneva, Switzerland.

[12] I.S. Gradshteyn and I.M. Ryzhik, Table of Integrals, Series, and Products, 5th ed., Academic Press, 1994.

[13] ATL-TILECAL-99-012 (ATL-COM-TILECAL-99-012), Simulation of the photomultiplier response, by: I. Fedorko, S.Tokar and I. Chirikov-Zorin - 19 May 1999, CERN

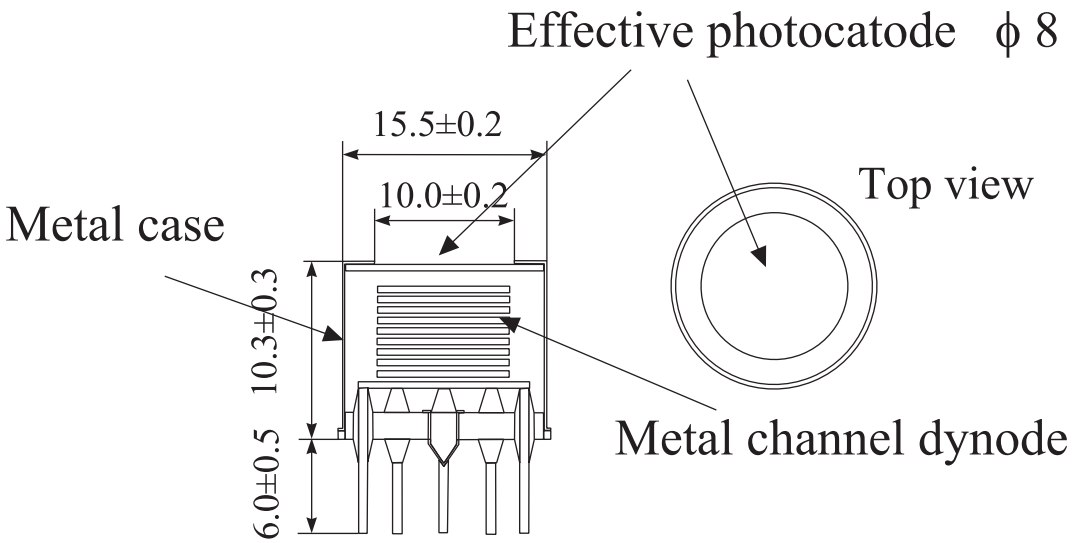

Figure 1: The overall view of a Hamamatsu R5600 photomultilier.

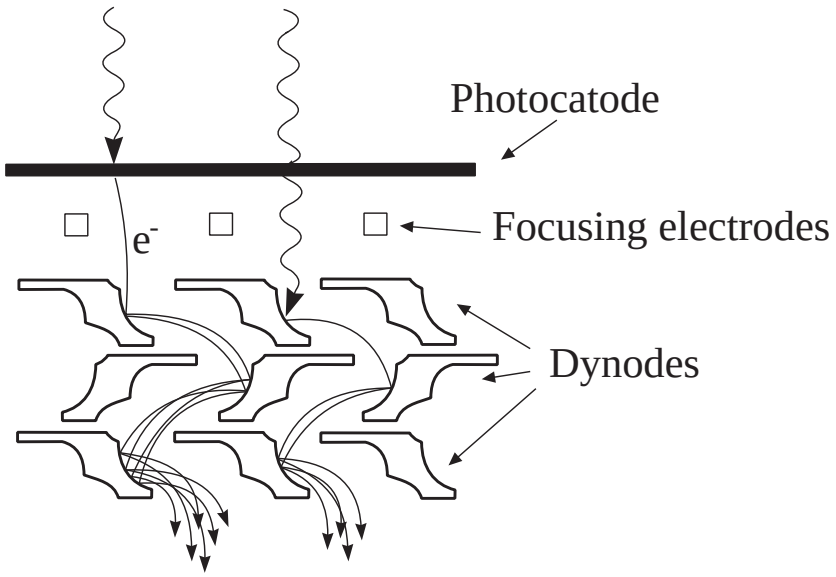

Figure 2: Charge multiplication process in the metal channel dynode photomultiplier.

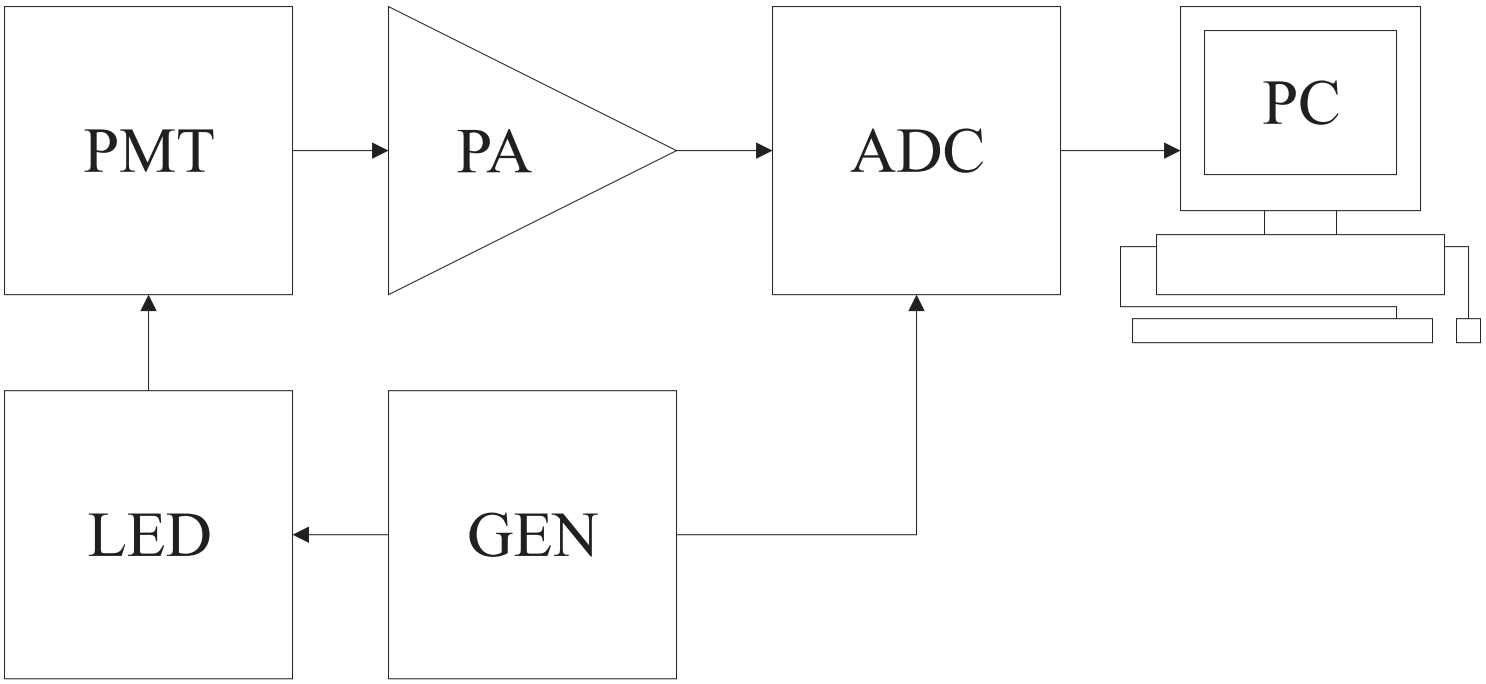

Figure 3: Block scheme of the experimental setup for the measurement of single photoelectron spectra.

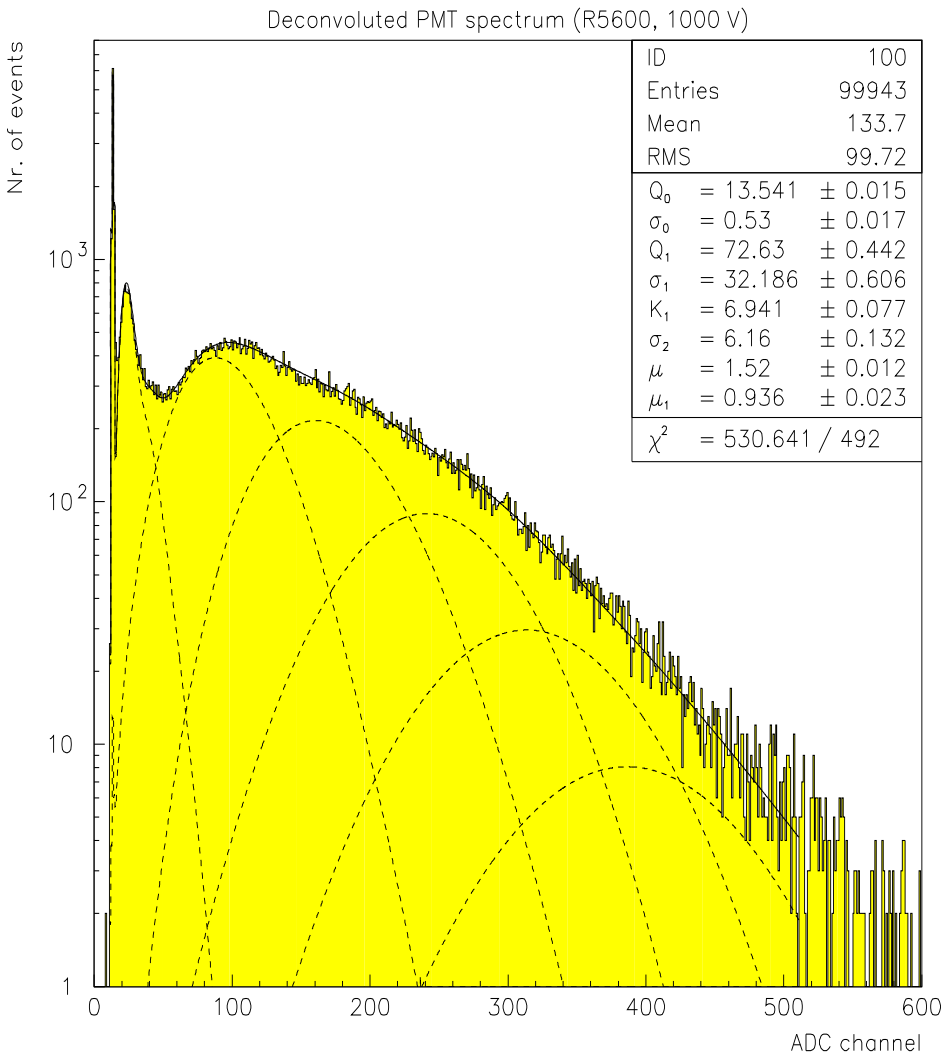

Figure 4: The deconvoluted LED spectrum taken at 1000 V by a Hamamatsu R5600 photomultilier.

The first dynode secondary emission coefficient K_1 is treated as an independent parameter.

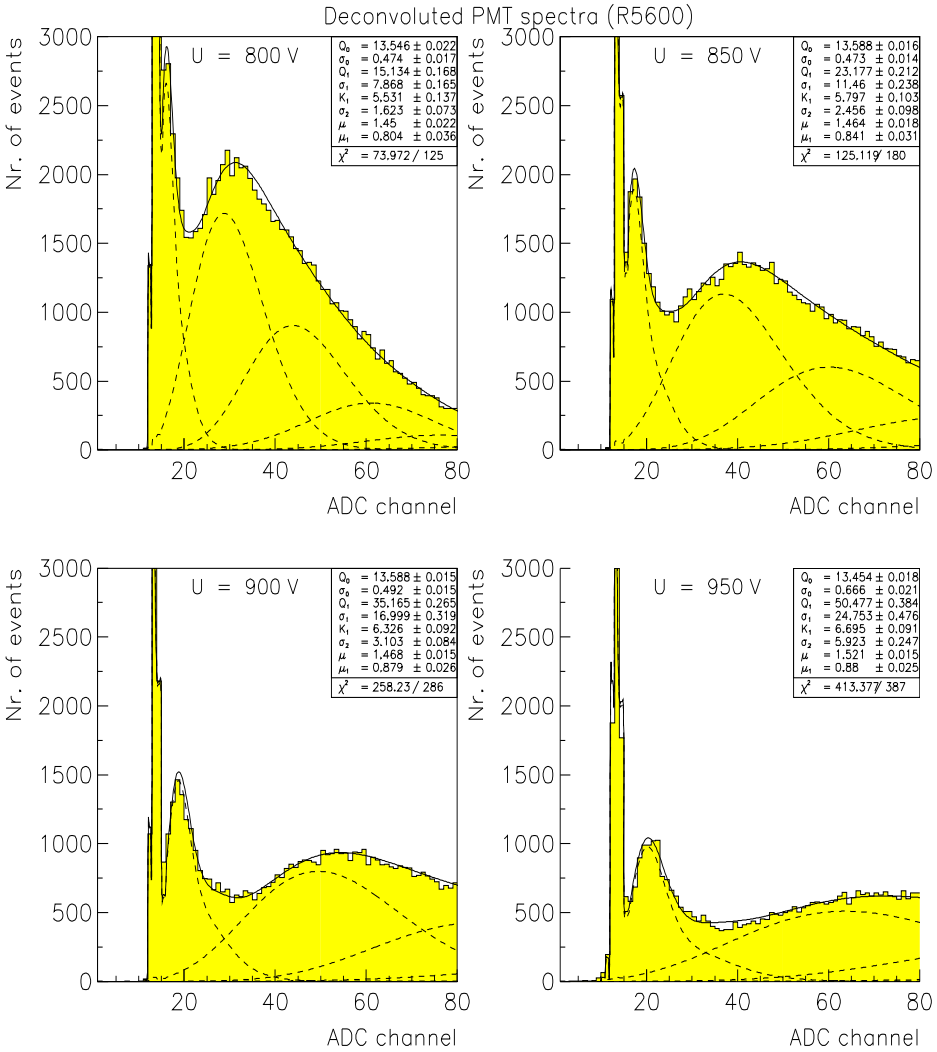

Figure 5: The deconvoluted LED spectra taken at 800 V, 850 V,900 V, and 950 V by a Hamamatsu R5600 photomultiplier. The same conditions are valid as in the case of the spectrum in Fig. 4.

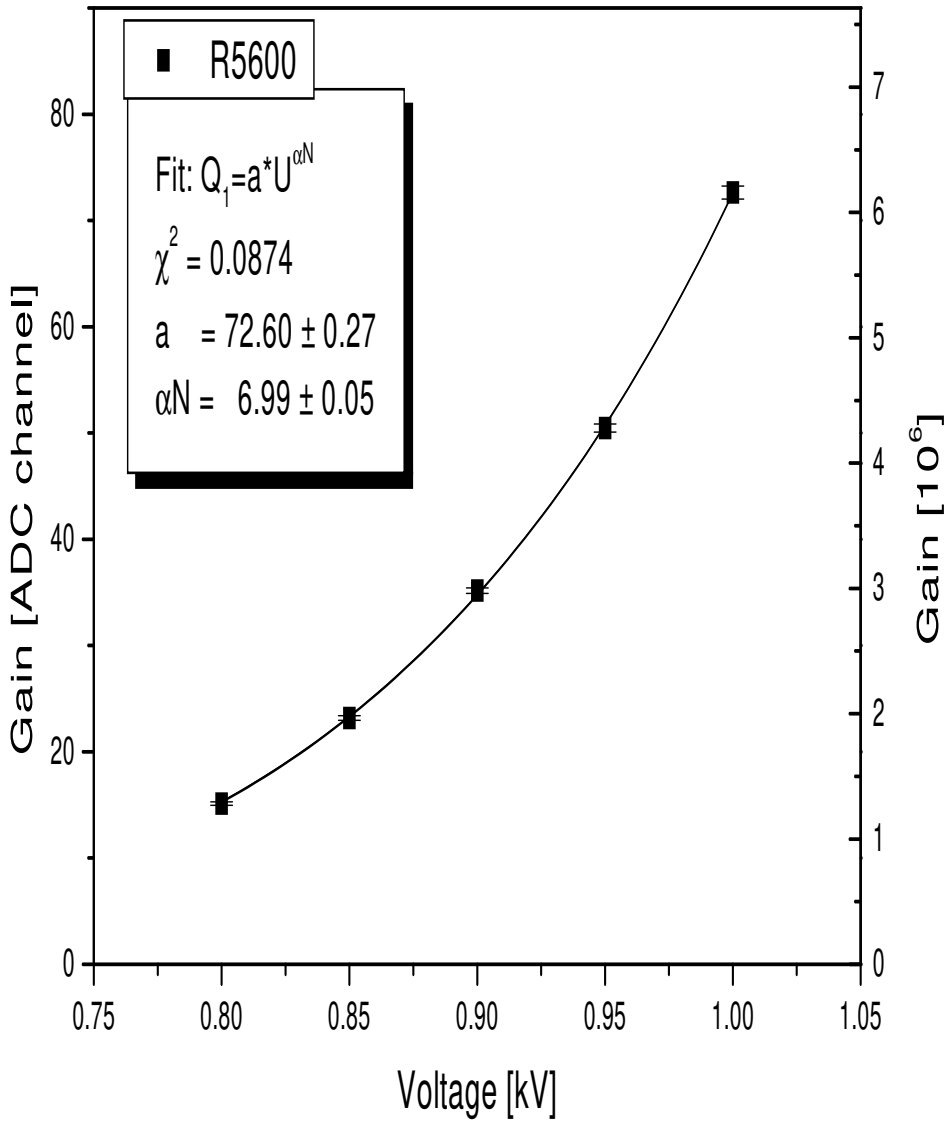

Figure 6: Dependencies of the gain (parameter Q_1) on voltage for the R5600 photomultiplier

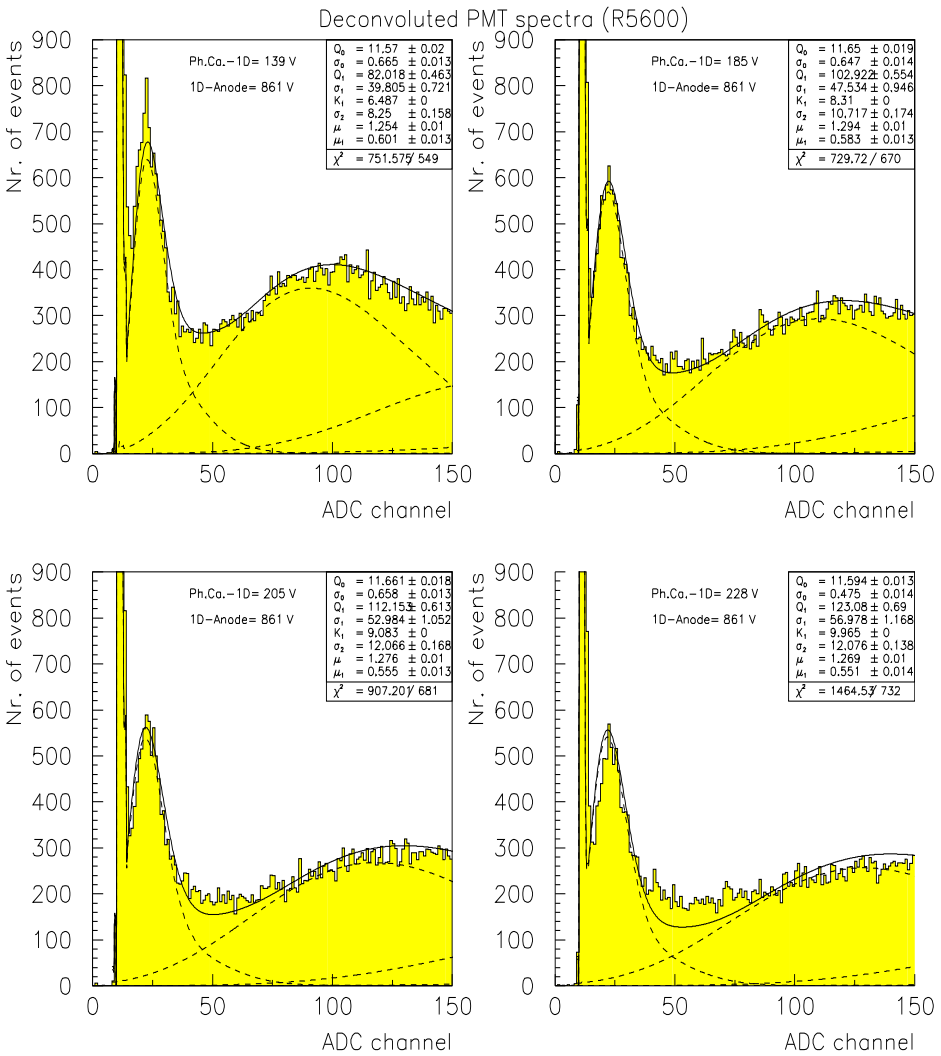

Figure 7: Deconvoluted LED spectra taken at different first dynode voltages (139 V, 185 V, 205 V, and 228V) by a Hamamatsu R5600. The voltage between the first dynode and anode was fixed at 861 V.

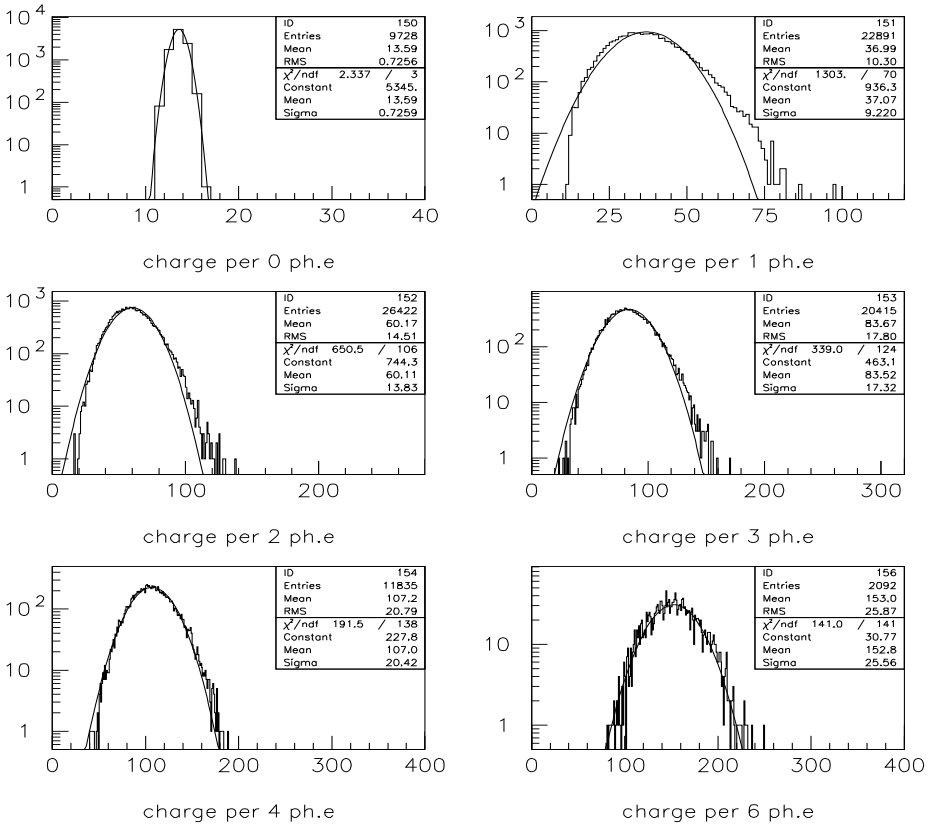

Figure 8: The simulated PMT responses at 850 V initiated by different number of photoelectrons - $n = 0, 1, 2, 3, 4$ and 6.

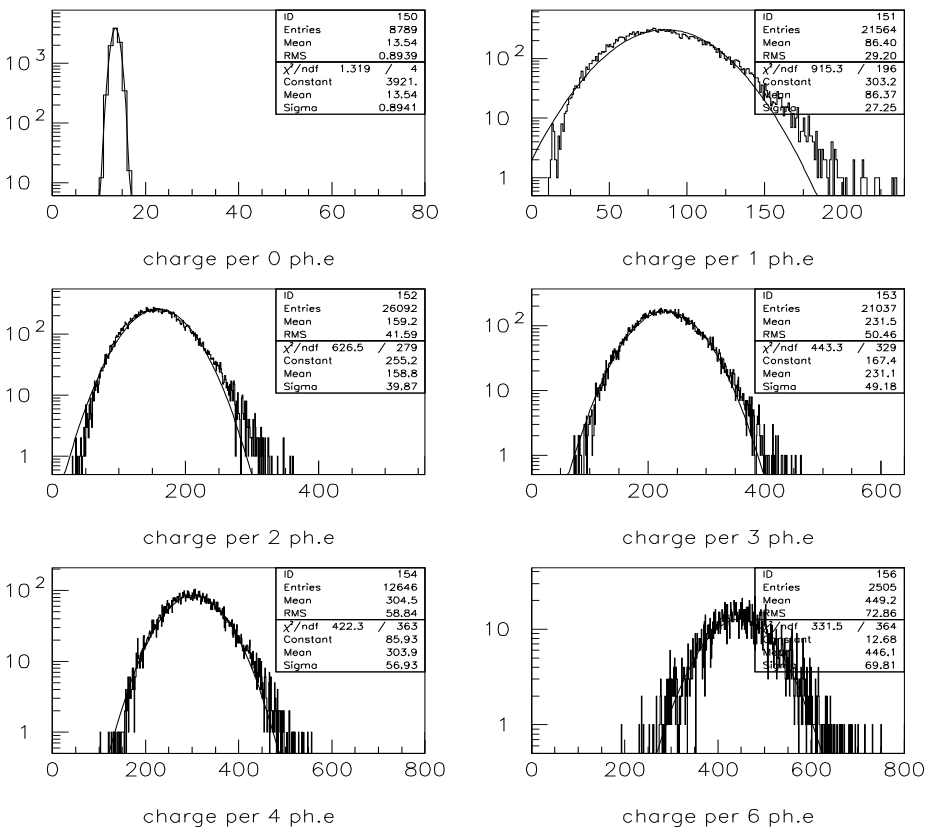

Figure 9: The simulated PMT responses at 1000 V initiated by different number of photoelectrons - $n = 0, 1, 2, 3, 4$ and 6.

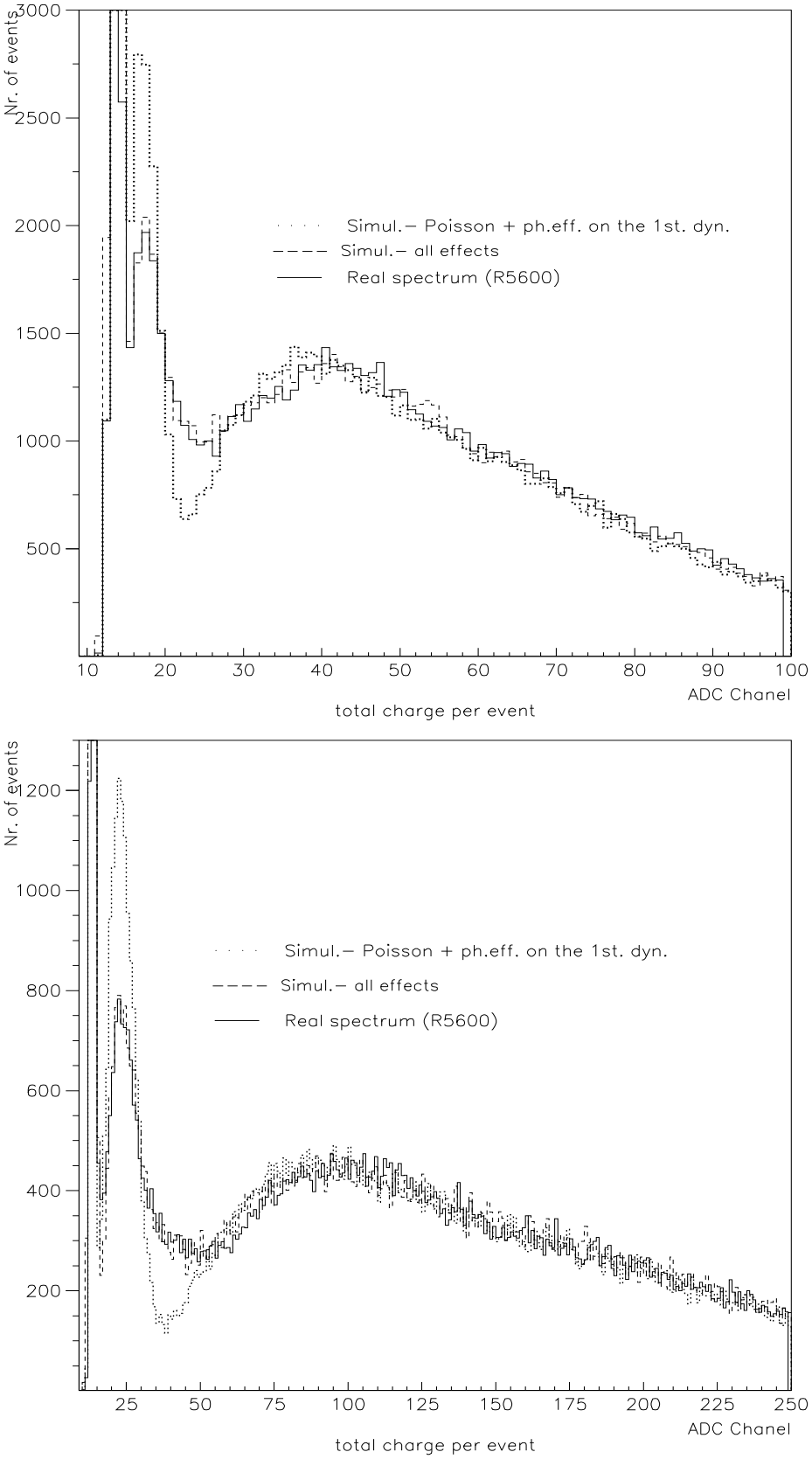

Figure 10: The spectra taken at 850 V and 1000 V taken by the R5600 PMT(black line) are compared with the simulated ones .